Chinese Journal of
POLYMER SCIENCE

RESEARCH ARTICLE

https://doi.org/10.1007/s10118-026-3817-0
Chinese J. Polym. Sci.

Edge-programmed Pentameric DNA Tetrahedra for Precision Drug Release through Stimuli-responsive Full-frame Disintegration

Chang-Qing Yang[a,†], Rui Song[a,†], Meng-Qiu Sun[a], Wei Luo[a], Wan-Mei Xie[a], Jin-Cheng Zeng[c*], Xin Liu[a,b*], and Hao Zhang[a*]

[a] *Guangdong Provincial Key Laboratory of Mathematical and Neural Dynamical Systems, School of Physical Sciences, Great Bay University, Dongguan 523000, China*
[b] *Basic Medical Institute of Ningxia Medical University, Yinchuan 750004, China*
[c] *Dongguan Key Laboratory of Medical Bioactive Molecular Developmental and Translational Research, Guangdong Provincial Key Laboratory of Medical Immunology and Molecular Diagnostics, Guangdong Medical University, Dongguan 523808, China*

Electronic Supplementary Information

Abstract Among the diverse DNA nanostructures explored for precise drug delivery, DNA tetrahedra have rapidly advanced to the forefront owing to their exceptional structural stability and highly efficient self-assembly. In contrast to conventional designs that rely on limited responsive elements, we engineered DNA tetrahedra that incorporate cytosine-rich sequences along every structural backbone. The acidic tumor microenvironment specifically triggers the stimuli-responsive full-frame disintegration of these nanocarriers. This complete structural collapse ensures the highly efficient and precise release of encapsulated antitumor drugs. Furthermore, assembling five tetrahedral units into a pentameric superstructure significantly enhanced drug payload capacity, improved cellular uptake, and maintained robust structural integrity. Systematic characterization confirmed the rapid stimulus-induced conformational transitions and selective cytotoxicity toward cancer cells. By effectively overcoming these fundamental delivery barriers, this study establishes practical design principles for the development of advanced DNA nanocarriers with higher therapeutic precision.

Keywords DNA nanocarriers; Stimuli-responsive; Conformational switching; Precision drug delivery; i-Motif

Citation: Yang, C. Q.; Song, R.; Sun, M. Q.; Luo, W.; Xie, W. M.; Zeng, J. C.; Liu, X.; Zhang, H. Edge-programmed pentameric DNA tetrahedra for precision drug release through stimuli-responsive full-frame disintegration. *Chinese J. Polym. Sci.* https://doi.org/10.1007/s10118-026-3817-0

INTRODUCTION

DNA nanotechnology has emerged as a distinctive platform for next-generation drug delivery systems. Conventional lipids, polymers, and inorganic nanocarriers can improve pharmacokinetics but often suffer from batch heterogeneity, limited addressability, and long-term toxicity or immunogenicity.[1,2] In contrast, DNA nanostructures are assembled by predictable base pairing, affording precise control of size, geometry, and ligand presentation, together with intrinsic biocompatibility, biodegradability, and easy integration of multiple targeting and stimuli-responsive modules into a single construct.[3,4] These features make DNA nanocarriers uniquely suited to encode complex behaviors such as tumor microenvironment–responsive release and multimodal targeting, which are difficult to systematically realize in other materials.[5–7]

* Corresponding authors, E-mail: zengjc@gdmu.edu.cn (J.C.Z.)
E-mail: liux@nxmu.edu.cn (X.L.)
E-mail: zhanghao@gbu.edu.cn (H.Z.)
† These authors contributed equally to this work.
Received May 26, 2026; Accepted July 19, 2026; Published online October 23, 2026

Within this class, tetrahedral DNA nanostructures/tetrahedral framework nucleic acids (TDNs/tFNAs) are prototypical DNA carriers. TDNs form in a one-pot step from four strands into mechanically robust, geometrically well-defined tetrahedra with high serum stability and resistance to nucleases.[8] Their compact 3D shape mediates efficient cellular uptake without transfection agents and favorable biodistribution, while vertices and edges provide multiple addressable sites for loading small-molecule drugs, nucleic acids, peptides, and imaging or targeting ligands.[9,10] As a result, TDN-based systems have been widely used for chemotherapy, gene therapy, imaging, and theranostics, often showing improved tumor accumulation and reduced systemic toxicity compared to free drugs and non-programmable carriers.[11,12]

The evolution of TDNs has followed a clear path, from static scaffolds to smart stimuli-responsive delivery systems. Early designs exploited the internal cavity to encapsulate doxorubicin or paclitaxel and simple surface ligands for receptor-mediated targeting.[8] More recent platforms integrate aptamers and tumor microenvironment–responsive motifs (pH, ATP, miRNA, enzymes) to achieve active targeting and on-demand drug release, as well as hybrid constructs where TDNs

© Chinese Chemical Society
Institute of Chemistry, Chinese Academy of Sciences

gate or decorate high-capacity cores such as metal–organic frameworks or hydrogels.[12–14] Nevertheless, most current systems rely on a few localized responsive elements, leading mainly to partial opening or gate detachment rather than complete structural disintegration, which can limit the drug release efficiency and payload capacity.[15–17] This gap has motivated the development of edge-programmed tetrahedral architectures that couple robust circulation stability with stimuli-triggered full-frame collapse for more precise and efficient drug liberation.

Responding to these limitations, we introduced distinctive edge-programmed pentameric DNA tetrahedra (illustrated in Fig. 1). Our design integrates cytosine-rich sequences throughout every structural backbone. The acidic tumor microenvironment directly triggers stimuli-responsive full-frame disintegration through i-motif conformational switching. The pentameric architecture provides four fundamental advantages over conventional monomeric tetrahedra: (1) substantially increased payload capacity by geometrically expanding the structural framework, thereby providing more available drug-loading sites; (2) multivalent targeting capability achieved through the dense, three-dimensional presentation of aptamers, creating stronger avidity effects that improve cellular recognition; (3) optimized structural dynamics, where the constrained mobility between tetrahedral units generates internal torsional stress that lowers the activation energy for pH-triggered disintegration; (4) improved cellular internalization through size optimization, where the assembled about 100 nm pentameric structure demonstrates significantly higher endocytic efficiency compared to individual about 40 nm tetrahedral units, while remaining below the threshold for enhanced permeability and retention (EPR) effects. These inherent characteristics established our platform as an innovative strategy for site-specific drug activation. This study defines practical design principles for advanced targeted drug delivery systems that minimize off-target effects and ultimately elevate therapeutic precision.

EXPERIMENTAL

Detailed experimental procedures, materials, synthesis, characterization, drug loading, drug release, cell experiments, and supplementary figures are provided in the electronic supplementary information (ESI).

RESULTS AND DISCUSSION

Design Rationale of the Edge-programmed DNA Tetrahedron for Full-frame Disintegration

We engineered a fundamental DNA tetrahedral building block to undergo complete structural collapse upon exposure to specific microenvironmental stimuli, as illustrated in Fig. 2. To achieve this full-frame disintegration, we embedded complementary C-rich (dashed lines in Fig. 2) and G-rich sequences (solid lines in Fig. 2) directly into the central double helix of all six structural edges. This configuration establishes a comprehensive network of microenvironment-triggered switches throughout the nanostructure framework. Unlike conventional strategies that confine responsive motifs to isolated vertices or single edges, our complete edge integration ensures that no rigid scaffold remains to entrap the encapsulated cargo after activation. The pervasive presence of six distinct C-rich segments distributed across the four strands is critical for achieving the simultaneous and complete dissociation of all six tetrahedral edges.

The core tetrahedron self-assembles from four rationally designed DNA strands (TDN-1, TDN-2, TDN-3, and TDN-4, as depicted in Fig. 2, upper panel). Each strand incorporates

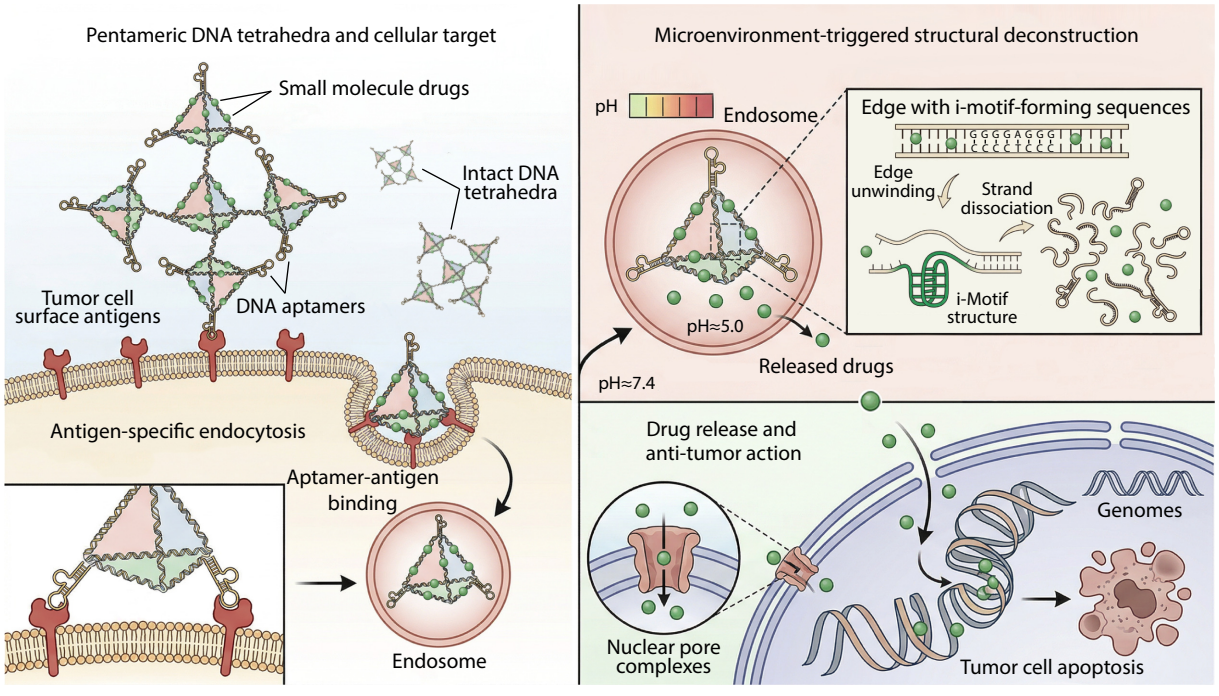


Fig. 1 Schematic illustration of the pentameric DNA tetrahedron enabling precision drug release *via* stimuli-responsive disintegration.

https://doi.org/10.1007/s10118-026-3817-0

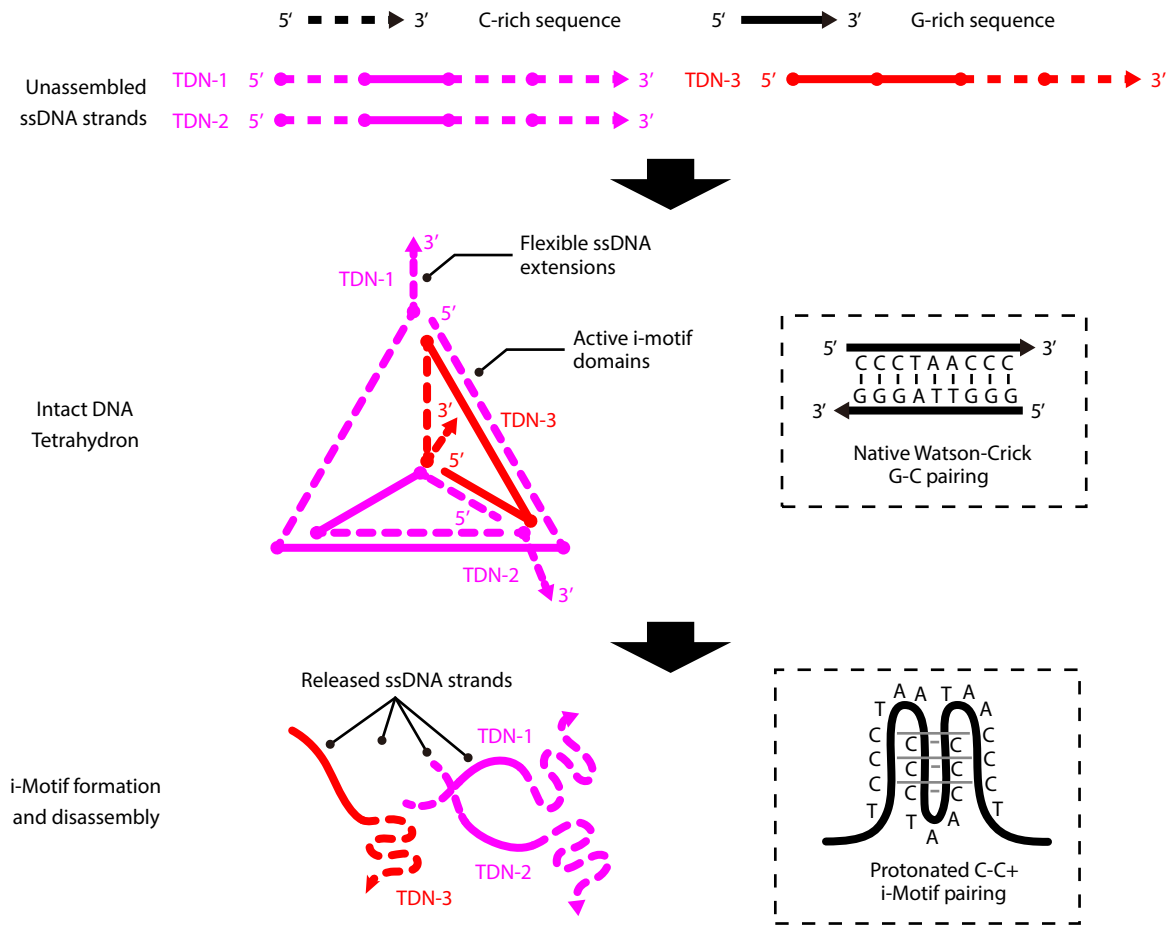


Fig. 2 Illustration of the edge-programmed DNA tetrahedron structure and its stimuli-responsive full-frame disintegration. Four single-stranded DNA components (TDN-1, TDN-2, TDN-3, TDN-4) self-assemble *via* sequence-specific hybridization into six double-stranded edges. Each edge incorporates stimuli-responsive C-rich segments (dashed lines) and complementary G-rich regions (solid lines). Flexible single-stranded extensions at the vertices fold to initiate i-motif conformational switching, link individual tetrahedra to construct the pentameric superstructure, and self-assemble into functional aptamers for targeted cellular recognition.

three primary C-rich or G-rich segments that form the structural backbone of the tetrahedron (the specific sequences are detailed in Table S1 in ESI). Two unpaired nucleotides were strategically inserted between structural segments in the sequence design. These hinge insertions ensure smooth geometric transitions at the tetrahedral vertices and maintain the structural integrity of all edges. Structural programming relies on a delicate thermodynamic balance between the stable double-stranded tetrahedral edges (Fig. 2, middle) and conditionally active i-motif domains (Fig. 2, lower part). We established an 18-nucleotide core length to maintain strict geometric rigidity during the systemic circulation. Concurrently, we extended the stimuli-responsive segments to lengths between 31 and 39 nucleotides. This specific length ratio provides a crucial mechanistic advantage, as the elongated C-rich domains generate a sufficient thermodynamic driving force upon protonation to actively disrupt the stable core. Meticulous sequence orthogonality was achieved to prevent unwanted spontaneous hybridization during the initial thermal annealing process.

To further optimize structural transformation kinetics, we appended flexible single-stranded extensions ranging from 13 to 21 nucleotides. Specifically, these extensions are located at the 3' ends of TDN-1, TDN-2, and TDN-3 and at the 5' end of TDN-4. These overhangs alleviate steric hindrance at highly crowded junctions and provide essential nucleation points to accelerate the transition into i-motif conformations. Furthermore, these accessible terminals provide modular attachment sites for two additional critical functions: mediating the hierarchical assembly of the pentameric superstructure and allowing self-assembly into functional aptamers for targeted cellular recognition. The combination of these flexible vertices and pervasive i-motif integration establishes the foundation for complete nanostructure disintegration, specifically within acidic tumor regions. This thorough collapse mechanism was designed to facilitate the unhindered release of the intercalated therapeutics. Ultimately, such an engineered response seeks to localize the structural breakdown exclusively at the target site and prevent premature drug leakage in healthy tissues.

Assembly and Structural Characterization of Pentameric DNA Tetrahedra

Conventional single DNA tetrahedra, although effective, exhibit certain inherent limitations for optimal drug delivery. Their rela-

https://doi.org/10.1007/s10118-026-3817-0

tively small molecular size restricts the total drug-loading capacity. The limited number of surface recognition sites can also hinder efficient cellular uptake, particularly when multiple nanostructures compete for entry. To overcome these constraints and significantly augment therapeutic efficacy, we developed a pentameric DNA tetrahedron architecture. This design comprises a central DNA tetrahedron acting as a core, surrounded by and connected to four peripheral DNA tetrahedra through the base pairing of flexible single-stranded extensions. This higher-order assembly was specifically engineered to enhance drug delivery efficiency by increasing both payload volume and multivalent targeting capabilities.

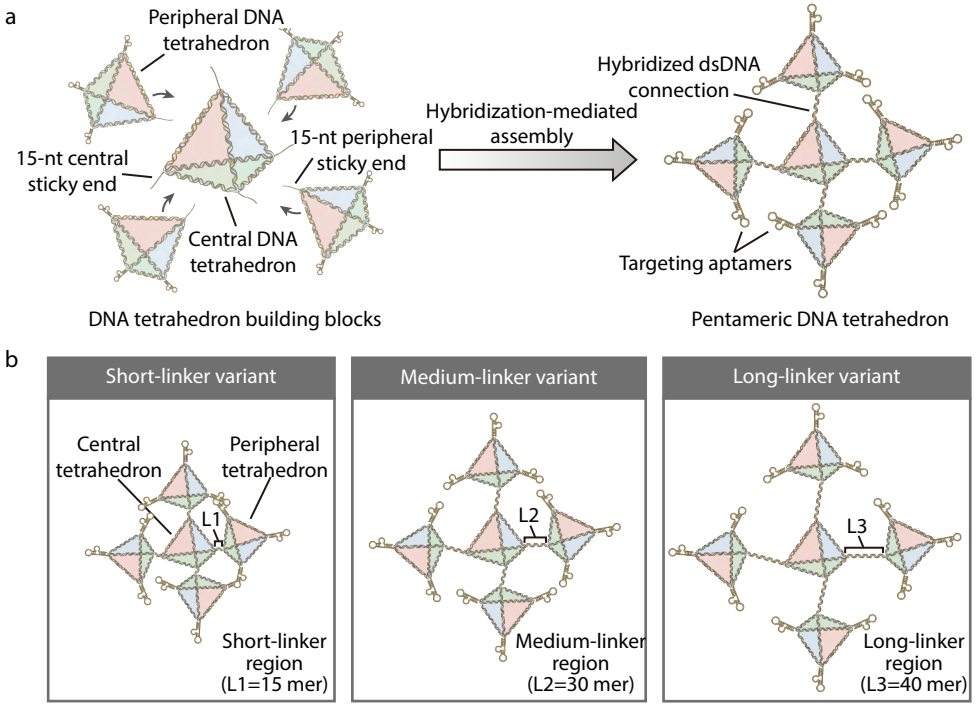
For this architecture, the central DNA tetrahedron was prepared with four identical 15-nt sticky ends extending from its vertices (Fig. 3a, Central Sticky Ends). Peripheral tetrahedra were modified to carry complementary sticky-end sequences on the flexible single-stranded extensions of their TDN-4 strands (Fig. 3a, Peripheral Sticky Ends). The single-stranded extensions of the TDN-1, TDN-2, and TDN-3 strands of these peripheral units were functionalized with specific Targeting Aptamers (Fig. 3a). In addition, through systematic adjustment of the linker sequence length connecting the central and peripheral tetrahedra, we generated three distinct pentameric configurations: a short-linker variant, medium-linker variant, and long-linker variant (Fig. 3b). This controlled structural diversity allowed for a comprehensive investigation of the optimal geometric arrangement for enhanced cellular uptake and precise drug delivery.

The synthesis of these nanostructures commenced with precise thermal annealing of individual DNA strands to form monomeric tetrahedra. The pentameric assembly was then proceeded by combining the pre-synthesized central and peripheral tetrahedra under carefully controlled conditions. Structural verification was performed by agarose gel electrophoresis and atomic force microscopy (AFM). Agarose gel electrophoresis (Figs. 3c and 3d) demonstrated clear migration patterns corresponding to the formation of dimeric, trimeric, and monomeric tetrahedral species. The distinct bands further confirm the successful assembly of all three pentameric configurations. Specifically, lane 3 in Fig. 3(c) shows a singular band for the monomeric tetrahedron, while lanes 2–4 in Fig. 3(d) verify the formation of the short-, medium-, and long-linker variants through specific hybridization. Complementary AFM imaging (Figs. 3e and 3f) provided a direct visualization of the assembled nanostructures, unequivocally resolving individual tetrahedra with dimensions of about 20 nm and larger pentameric assemblies measuring about 80 nm. These characterization data establish the structural integrity and efficient assembly of the pentameric DNA tetrahedra.

Extracellular Validation of Stimuli-responsive Disintegration

Fluorescence spectroscopy with thiazole orange and circular dichroism spectroscopy were used to analyze the conformational changes and secondary structure transitions. Thiazole orange exhibits distinctive fluorescence properties that highly depend on its specific binding environment.[18] The intercalation of rigid double-stranded DNA edges partially restricts molecular rotation and generates moderate fluorescence enhancement. Conversely, binding to the compact i-motif imposes severe steric constraints. This tight binding completely suppresses nonradiative decay pathways and significantly amplifies the overall fluorescence intensity.[19,20]

The mildly acidic tumor microenvironment acts as a critical trigger for precise drug delivery systems. To systematically characterize the structural dynamics of edge-programmed DNA tetrahedra under physiologically relevant conditions, we



https://doi.org/10.1007/s10118-026-3817-0

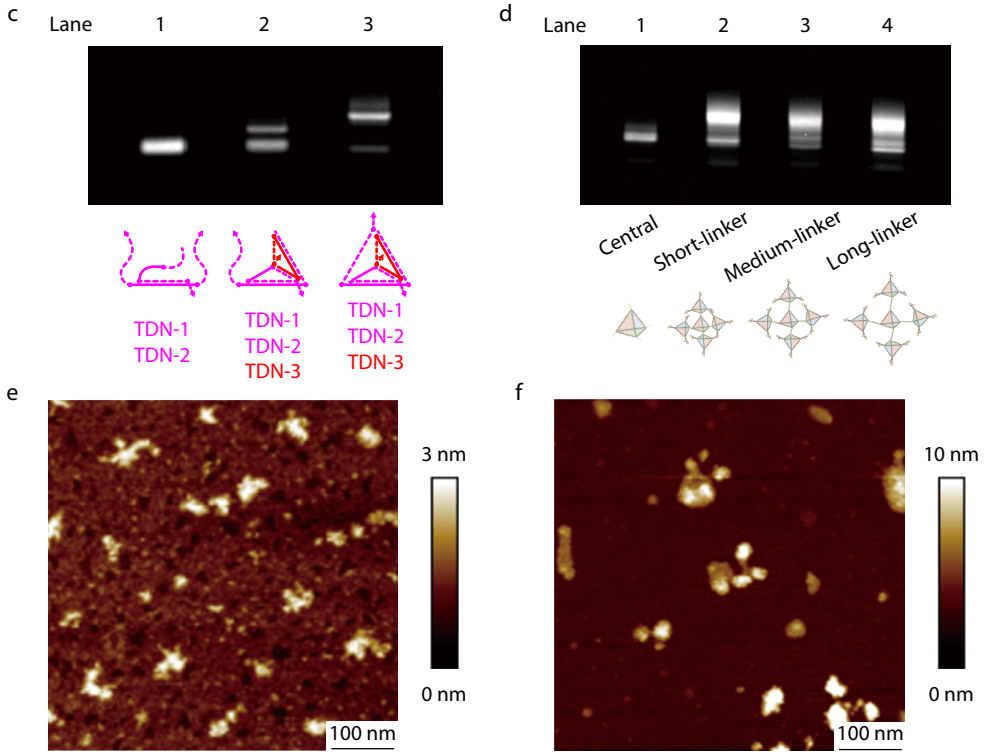


Fig. 3 Synthesis and structural characterization of the monomeric DNA tetrahedra and pentameric superstructures. (a) Assembly strategy for constructing peripheral DNA tetrahedra from individual DNA tetrahedron building blocks; (b) Structural variants of pentameric assemblies featuring different spacer lengths; (c) Agarose gel electrophoresis analysis of the assembly intermediates. Lane 1: DNA dimers composed of TDN-1 and TDN-2 at a 1:1 molar ratio. Lane 2: DNA trimers formed by TDN-1, TDN-2, and TDN-3 at an equimolar ratio. Lane 3: assembled monomeric DNA tetrahedra comprising all four strands at an equimolar ratio. (d) Validation of pentamer formation. Lane 1: central DNA tetrahedra. Lanes 2–4: assemblies of the short-linker, medium-linker, and long-linker pentameric variants respectively. All gels were stained with ethidium bromide and imaged under ultraviolet illumination. (e) Atomic force microscopy image of individual tetrahedra exhibiting a monomeric diameter of approximately 40 nm. (f) Atomic force microscopy image of the pentameric assemblies revealing an overall superstructure diameter of approximately 100 nm.

evaluated the nanostructures on a pH gradient ranging from 5.0 to 7.4. Fig. 4(a) demonstrates that after DNA tetrahedral incubation in buffer solutions with different pH values, the fluorophore-bound tetrahedra at pH=5.0 exhibits maximal fluorescence intensity. This strong signal is consistent with complete structural reorganization into i-motif conformations. Intermediate acidic conditions between pH=5.5 and 6.0, produced graded fluorescence responses. The physiological stability of our pentameric DNA tetrahedra is derived from their unique structural design. The dense three-dimensional framework provides steric protection against nuclease degradation, consistent with established findings that tetrahedral DNA nanostructures exhibit enhanced resistance to DNase I.[8] Furthermore, the combination of mechanically rigid tetrahedral units (persistence length about 40 nm) and programmed sticky-end hybridization through relatively long (15-nt) connections ensures structural integrity under physiological conditions, which is consistent with recent advances demonstrating that DNA assemblies can achieve both circulatory stability and microenvironment-responsive behavior.[11] The time-resolved fluorescence kinetics (Fig. 4b) further elucidated the full-frame disintegration process. Acidic buffers induced rapid signal amplification within the first 8 h and reached a plateau at 12 h, signifying a complete structural collapse. At physiological pH (7.4), the fluorescence intensity exhibited no significant increase throughout the observation period. This stability indicates that the edge-programmed nanostructures maintained their original double-stranded framework without any detectable disassembly.

Circular dichroism spectroscopy provided direct evidence for these secondary structure transitions (Fig. 4c). Spectra recorded at pH=7.4 displayed canonical B-form DNA signatures characterized by a negative peak at 240 nm and a positive peak at 280 nm. The introduction of acidic conditions induces distinct spectral shifts. A new positive peak emerged at 245 nm along with a second positive band at 290 nm. The quantitative drug release results (Fig. 4d, Figs. S1 and S2 in ESI) confirm pH-responsive behavior: acidic conditions triggered substantial doxorubicin release (41.0% at pH=5.5), while the constructs remained highly stable at physiological pH (4.5% at pH=7.4). Release follows a sustained 24-h profile, consistent with gradual nanostructure disassembly during the pH transition, which helps maintain therapeutic drug levels in tumor tissue. These combined spectral changes definitively confirmed the formation of the i-motif structures. This validation established an unambiguous correlation between microenvironment-triggered full-frame disintegration and measurable conformational switching. The gradual pH-dependent transition observed in our system likely arises from the distributed i-motif-forming sequences throughout the nanostructure framework combined with microenvironmental variations within the pentameric assembly. While this

https://doi.org/10.1007/s10118-026-3817-0

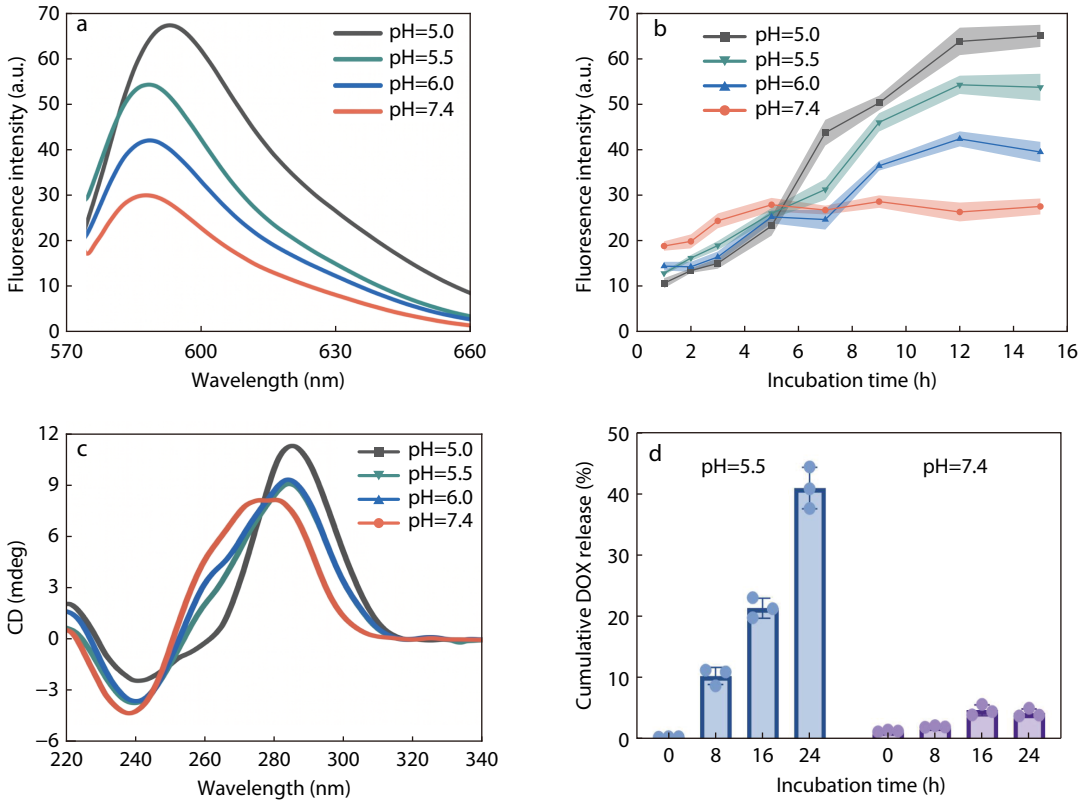


Fig. 4 Stimuli-responsive structural transitions of the edge-programmed DNA tetrahedra. (a) Fluorescence intensity of thiazole orange-bound DNA tetrahedra after 12 h incubation in buffers of ranging from acidic environments to physiological conditions; (b) Time-dependent fluorescence evolution of thiazole orange-bound DNA tetrahedra in acidic environments and physiological conditions; (c) Circular dichroism spectra confirming the disintegration through distinct B-DNA to i-motif conformational shifts; (d) Time-dependent doxorubicin release from pentameric DNA tetrahedra at pH=5.5 and 7.4. Error bars represent standard deviation (n=3).

progressive response differs from the sharp all-or-none transitions reported in some simpler DNA switches, it may provide better adaptation to the heterogeneous pH gradients found in actual tumor microenvironments.

Structural Determinants for Optimal Full-frame Disintegration

To evaluate the structural features governing efficient full-frame disintegration, we engineered systematic variations of the edge-programmed tetrahedron (detailed oligonucleotide sequences are given in Table S3 in ESI). The primary design integrates C-rich sequences across all six edges along four flexible vertex extensions and is designated as a hexa-responsive construct. We compared this architecture to restricted designs possessing only four or two C-rich edges, termed tetra-responsive and di-responsive constructs, respectively. We also evaluated a nonresponsive control lacking all C-rich domains and a vertex-locked variant that contains six C-rich edges but lacks flexible terminal extensions. Agarose gel electrophoresis confirmed the successful synthesis of each architectural variant, as depicted in Fig. S3 (in ESI).

Subsequent fluorescence assays demonstrated that only architectures integrating both C-rich edges and flexible free ends exhibited stimuli-responsive signal enhancements. Fig. 5(a) shows that the hexa-responsive construct generated the strongest conformational response. The tetra-responsive and di-responsive designs produced sequentially weaker responses, as shown in Figs. 5(b) and 5(c), respectively. This behavior establishes a definitive correlation between the number of responsive edges and structural disintegration efficiency. The non-responsive control shown in Fig. 5(d) verifies the absolute necessity of C-rich sequences for acidic activation. Crucially, the vertex-locked variant analyzed in Fig. 5(e) failed to respond, proving that flexible free ends remain critical, even when all six edges inherently possess conformation-switching capabilities. These comparative results (Fig. 5f) indicate that optimal full-frame disintegration requires both comprehensive edge programming and flexible free-ends. The unresponsiveness of the vertex-locked variant confirms that these free terminals serve as indispensable nucleation points for overcoming the kinetic barriers of protonation-induced transitions within the constrained tetrahedral framework.

Enhanced Cellular Targeting and Precision Drug Delivery of Multivalent Superstructures

We conducted cellular studies to evaluate the targeting specificity and precision of drug delivery efficiency of the engineered nanostructures. This evaluation compared the monomeric tetrahedral DNA nanostructure TDN against the three pentameric variants identified as PTDN-S (short-linker variant), PTDN-M (medium-linker variant), and PTDN-L (long-linker variant). We used MCF-7 human breast cancer cells and normal MCF-10A mammary epithelial cells for these comparative assays. All constructs incorporated MUC1-specific DNA aptamers

https://doi.org/10.1007/s10118-026-3817-0

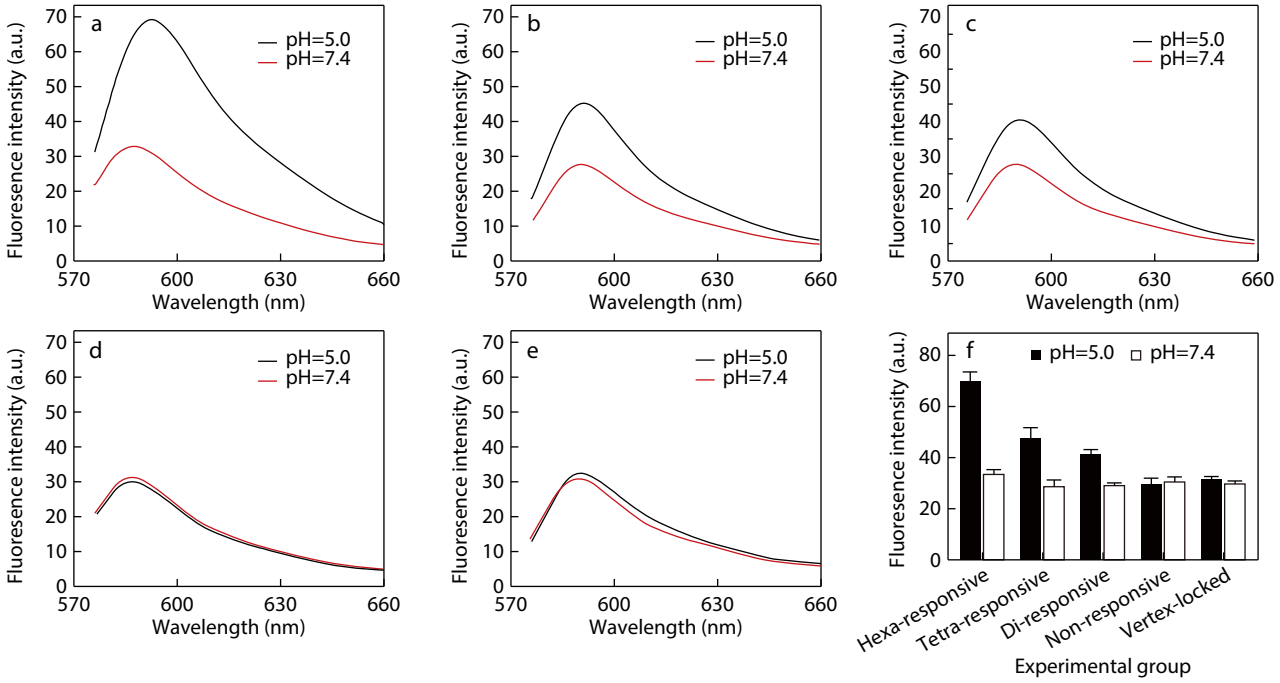


Fig. 5 Stimuli-responsive fluorescence spectra of the engineered DNA tetrahedron variants. Black curves represent acidic conditions at pH=5.0 and red curves indicate physiological conditions at pH=7.4. (a) The hexa-responsive construct integrates six active edges with flexible free ends to produce a maximal conformational response; (b) The tetra-responsive variant contains four active edges and exhibits an intermediate signal enhancement; (c) The di-responsive variant contains two active edges and exhibits a significantly reduced response; (d) The non-responsive control entirely lacks active edges and shows negligible changes; (e) The vertex-locked variant possesses six active edges but lacks flexible free ends and similarly reveals no distinct stimuli responsive differences; (f) Quantitative comparison of the maximum fluorescence intensities recorded at 590 nm of all ten experimental groups. Error bars represent standard deviations.

(detailed sequences are provided in Table S2 in ESI) at strategic vertex positions to enable active cellular recognition. The monomeric architecture contains four distributed aptamers. The pentameric superstructures arrayed 12 aptamers to achieve multivalent targeting. Doxorubicin (Dox) was selected as a model therapeutic agent because of its intrinsic fluorescence. Intercalation of the drug into stable double-stranded edges resulted in optimized loading capacities of about 20 doxorubicin molecules per monomeric TDN and about 100 molecules per pentameric assembly.

Confocal microscopy revealed three critical findings regarding cellular interactions. Control experiments with free doxorubicin demonstrated equivalent and non-specific uptake in both cell types (Fig. S4 in ESI), confirming the absolute necessity of targeted delivery systems. Subsequent assays were performed to evaluate the aptamer-modified TDN-Dox conjugates. These monomeric carriers exhibited selective accumulation exclusively within the MCF-7 cancer cells, as illustrated in Fig. 6(a). Furthermore, pentameric architectures displayed significantly superior performance characteristics. As shown in Figs. S5 and S6 (in ESI), the short-linker variant PTDN-S generated the most intense intracellular fluorescence signals among all tested assemblies. Quantitative analysis performed at equivalent therapeutic doses of Dox (5 μmol/L) demonstrated a substantial enhancement in targeted delivery. Fig. 6(b) and Fig. S7 (in ESI) show that the PTDN-S superstructure achieved about 3.7-fold greater intracellular drug accumulation compared to the monomeric TDN platform. Flow cytometry quantification (Fig. S8 in ESI) confirmed the confocal microscopy observations, with PTDN-S showing significantly higher cellular uptake compared to monomeric TDN, directly demonstrating the targeting advantage of the multivalent pentameric architecture.

The superior intracellular efficacy of pentameric superstructures originates from multi-faceted structural enhancements. The dense presentation of 12 aptamers significantly amplified target recognition through multivalent avidity compared with the monomeric building block. Concurrently, an expanded nanoscale diameter promotes more robust endocytic internalization. Furthermore, the constrained mobility between the assembled tetrahedral units generates internal torsional stress. This mechanical tension lowers the thermodynamic barrier for strand dissociation and accelerates the simultaneous i-motif conformational switching to ensure rapid full-frame disintegration. Finally, the superior delivery performance of the compact PTDN-S variant over the PTDN-M and PTDN-L designs confirms that a tighter geometric organization optimally balances the systemic circulation stability with efficient stimuli-responsive disassembly.

Systematic Assessment of Therapeutic Efficacy and Selectivity

Cytotoxicity studies were conducted to evaluate the therapeutic potential and cancer selectivity of our DNA nanostructure-based drug delivery systems. Using MTT assays after 48-h co-culture periods, we compared free doxorubicin with TDN-Dox and PTDN-Dox. These comparisons were performed at equivalent concentrations of 1 and 5 μmol/L doxorubicin in both MCF-10A normal mammary cells and MCF-7 breast cancer cells.

Dose-dependent cytotoxicity was consistently observed in

https://doi.org/10.1007/s10118-026-3817-0

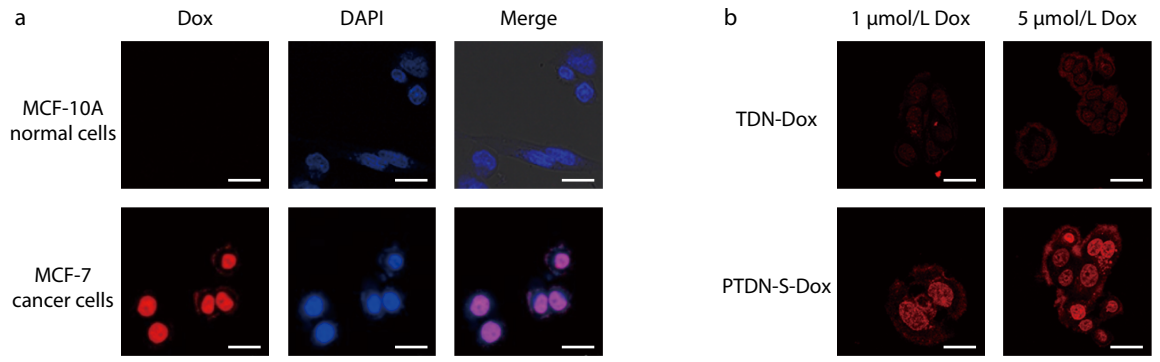


Fig. 6 Targeted delivery of doxorubicin using aptamer-modified DNA nanostructures. (a) Confocal microscopy image of MCF-10A normal mammary epithelial cells (upper panel) and MCF-7 breast cancer cells (lower panel) treated with TDN-Dox at 1 μmol/L doxorubicin equivalent concentration; (b) Comparative drug delivery efficiency between monomeric (upper panel) and pentameric DNA nanostructures (lower panel). Confocal microscopy image of MCF-7 breast cancer cells treated with TDN-Dox or PTDN-S-Dox at 1 μmol/L (left) or 5 μmol/L (right) doxorubicin equivalent concentration, respectively. Blue indicates DAPI staining of nuclei and DNA nanostructures. Red indicates doxorubicin fluorescence. Scale bars: 30 μm.

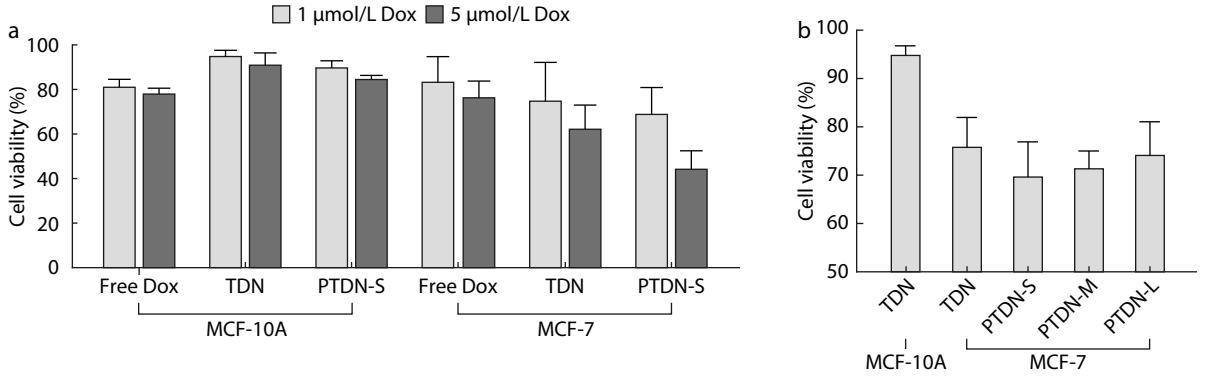


Fig. 7 Comparative cytotoxicity of DNA nanostructure-drug conjugates. (a) MCF-10A normal mammary cells and MCF-7 breast cancer cells treated with free Dox, TDN-Dox, or PTDN-Dox at 1 μmol/L doxorubicin (light gray) and 5 μmol/L doxorubicin (dark gray) concentrations; (b) Linker length-dependent cytotoxicity at a fixed 1 μmol/L doxorubicin concentration. Group 1: the monomeric TDN. Group 2: the short-linker PTDN-S variant. Group 3: the medium-linker PTDN-M variant. Group 4: the long-linker PTDN-L variant. Data represent mean values with standard deviations from three independent experiments.

all formulations. Specifically, five micromolar treatments, including free doxorubicin, TDN-Dox, and PTDN-Dox complexes, significantly reduced cell viability compared with their micromolar counterparts (Fig. 7a). Cytotoxicity assessment revealed distinct patterns of cancer cell selectivity across different formulations. Although free doxorubicin showed cytotoxicity comparable to that of PTDN-S-Dox in normal MCF-10A cells, the pentameric nanostructure demonstrated significantly enhanced anticancer efficacy in MCF-7 cells (particularly at 5 μmol/L), highlighting its improved therapeutic index through selective cancer cell targeting. In contrast to the non-specific cytotoxicity of conventional drug delivery methods, both TDN-Dox and PTDN-Dox complexes exhibited preferential toxicity toward MCF-7 cancer cells over normal mammary cells (Fig. 7b). The pentameric PTDN formulation consistently elicited stronger cytotoxic effects than those of the monomeric TDN system at equivalent drug concentrations, confirming its superior delivery efficiency. This observed selectivity pattern aligns well with the cellular uptake observations reported, and strongly supports the precise targeting capability of our aptamer-functionalized DNA nanostructures. A linker-length dependency study (Fig. 7b) further demonstrated that the short-linker pentameric variant PTDN-S generated the strongest cytotoxic effects. This was followed by the medium-linker PTDN-M and the long-linker PTDN-L variants. This performance gradient indicates that the optimal intertetrahedral spacing is critical. It must balance the structural stability during systemic circulation with efficient intracellular drug release. Both overly extended linkers and excessively compact designs can compromise therapeutic efficacy.

CONCLUSIONS

In this study, we developed edge-programmed pentameric DNA tetrahedra for precise drug delivery. These nanostructures integrate C-rich sequences along every structural backbone, achieving stimuli-responsive full-frame disintegration through i-motif conformational switching in the acidic tumor microenvironment. This thorough structural collapse ensures the highly efficient and precise release of encapsulated therapeutics. Pentameric assembly enhances drug payload capacity and provides multivalent targeting for robust cellular uptake, while concurrently preserving structural integrity. Such an advanced system directly addresses the critical challenges in payload capacity, targeting efficiency, and responsive release inherent to DNA

https://doi.org/10.1007/s10118-026-3817-0

nanocarriers. This study establishes valuable design principles for advanced DNA nanocarriers, thereby directly supporting the engineering of more effective and precise tumor-targeted therapeutic platforms.

Conflict of Interests

The authors declare no interest conflict.

Electronic Supplementary Information

Electronic supplementary information (ESI) is available free of charge in the online version of this article at http://doi.org/10.1007/s10118-026-3817-0.

Data Availability Statement

The original contributions of this study are included in the article and supplementary materials. Further inquiries can be directed toward the corresponding authors.

ACKNOWLEDGMENTS

This work was financially supported by the National Natural Science Foundation of China (No. 22405031), Guangdong Provincial Introduction Program (No. 2023QN10Y105), Guangdong Basic and Applied Basic Research Foundation (No. 2026A1515012001), Open Research Fund of Songshan Lake Materials Laboratory (No. 2023SLABFN28), and GBU-CINEHAI Joint PoC Laboratory for Medicinal Bioactive Substances.

REFERENCES

1 Ullah, M.; Shah, M. I.; Hasan, M. W.; Jamshed, M.; Mustafa, U.; Inam, M. Engineered metal nanoparticles for precision drug delivery: pioneering the future of medicine: mini review. *J Chin. Chem. Soc.* **2024**, *71*, 1358–1367.
2 Liu, S.; Zheng, Y.; Pan, L.; Wang, W.; Li, Y.; Liu, Z.; Zhang, X. Nanodelivery of nucleic acids for plant genetic engineering. *Discover Nano* **2025**, *20*, 31.
3 Li, S.; Xu, M.; Yao, C.; Yang, D. DNA-Based nanostructures for tumor microenvironment-responsive drug delivery. *Adv. Drug Deliv. Rev.* **2025**, *223*, 115610.
4 Li, C.; Wang, M.; Li, P.-F.; Sheng, J.; Fu, Q. Construction of smart DNA-based drug delivery systems for cancer therapy. *Small* **2024**, *20*, 2306257.
5 He, S.; Fan, T.; Wang, Y.; Wei, C.; Hu, J. Recent advances in DNA nanostructure-enabled drug delivery. *ChemNanoMat* **2023**, *9*, e202200459.
6 Zhang, T.; Tian, T.; Zhou, R.; Li, S.; Ma, W.; Zhang, Y.; Liu, N.; Shi, S.; Li, Q.; Xie, X.; Ge, Y.; Liu, M.; Zhang, Q.; Lin, S.; Cai, X.; Lin, Y. Design, fabrication and applications of tetrahedral DNA nanostructure-based multifunctional complexes in drug delivery and biomedical treatment. *Nat. Protoc.* **2020**, *15*, 2728–2757.
7 Tang, W.; Liu, J.; Ding, B. Nucleic acid nanostructure for delivery of CRISPR/Cas9-based gene editing system. *Interdiscip. Med.* **2023**, *1*, e20220014.
8 Copp, W.; Pontarelli, A.; Wilds, C. J. Recent advances of DNA tetrahedra for therapeutic delivery and biosensing. *ChemBioChem* **2021**, *22*, 2237–2246.
9 Ouyang, Y.; Zhang, P.; Willner, I. DNA tetrahedra as functional

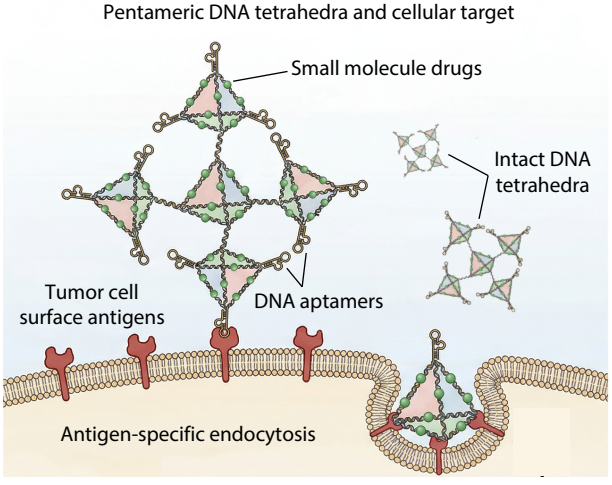
Graphical Abstract

Edge-programmed Pentameric DNA Tetrahedra for Precision Drug Release through Stimuli-responsive Full-frame Disintegration

Chang-Qing Yang, Rui Song, Meng-Qiu Sun, Wei Luo, Wan-Mei Xie, Jin-Cheng Zeng, Xin Liu, and Hao Zhang

Great Bay University; Basic Medical Institute of Ningxia Medical University; Guangdong Medical University

Stimuli-responsive DNA tetrahedra release drugs in tumors by acidic-triggered breakdown. This multivalent design boosts payload capacity and uptake while ensuring precise cancer-targeted therapy.



nanostructures: from basic principles to applications. *Angew. Chem. Int. Ed.* **2024**, *63*, e202411118.
10 Li, J.; Yan, R.; Shi, S.; Lin, Y. Recent progress and application of the tetrahedral framework nucleic acid materials on drug delivery. *Expert Opin. Drug Deliv.* **2023**, *20*, 1511–1530.
11 Sharma, A.; Vaswani, P.; Bhatia, D. Revolutionizing cancer therapy using tetrahedral DNA nanostructures as intelligent drug delivery systems. *Nanoscale Adv.* **2024**, *6*, 3714–3732.
12 Tian, T.; Zhang, T.; Shi, S.; Gao, Y.; Cai, X.; Lin, Y. A dynamic DNA tetrahedron framework for active targeting. *Nat. Protoc.* **2023**, *18*, 1028–1055.
13 Zhang, P.; Ouyang, Y.; Sohn, Y. S.; Nechushtai, R.; Pikarsky, E.; Fan, C.; Willner, I. pH- and miRNA-responsive DNA-tetrahedra/metal–organic framework conjugates: functional sense-and-treat carriers. *ACS Nano* **2021**, *15*, 6645–6657.
14 Lee, Y.; Nam, K.; Kim, Y. M.; Yang, K.; Kim, Y.; Oh, J.-W.; Roh, Y. H. Functional polymeric DNA nanostructure-decorated cellulose nanocrystals for targeted and stimuli-responsive drug delivery. *Carbohydr. Polym.* **2024**, *340*, 122270.
15 Wang, T.; Liu, Y.; Wu, Q.; Lou, B.; Liu, Z. DNA nanostructures for stimuli-responsive drug delivery. *Smart Mater. Med.* **2022**, *3*, 66–84.
16 Seitz, I.; Shaukat, A.; Nurmi, K.; Ijäs, H.; Hirvonen, J.; Santos, H. A.; Kostiainen, M. A.; Linko, V. Prospective cancer therapies using stimuli-responsive DNA nanostructures. *Macromol. Biosci.* **2021**, *21*, 2100272.
17 Kim, T.; Nam, K.; Kim, Y. M.; Yang, K.; Roh, Y. H. DNA-assisted smart nanocarriers: progress, challenges, and opportunities. *ACS Nano* **2021**, *15*, 1942–1951.
18 Lubitz, I.; Zikich, D.; Kotlyar, A. Specific high-affinity binding of thiazole orange to triplex and G-quadruplex DNA. *Biochemistry* **2010**, *49*, 3567–3574.
19 Sheng, Q.; Neaverson, J. C.; Mahmoud, T.; Stevenson, C. E. M.; Matthews, S. E.; Waller, Z. A. E. Identification of new DNA i-motif binding ligands through a fluorescent intercalator displacement assay. *Org. Biomol. Chem.* **2017**, *15*, 5669–5673.
20 Kang, B. H.; Gao, Z. F.; Li, N.; Shi, Y.; Li, N. B.; Luo, H. Q. Thiazole orange as a fluorescent probe: label-free and selective detection of silver ions based on the structural change of i-motif DNA at neutral pH. *Talanta* **2016**, *156*, 141–146.